Journal of Structural Geology 33 (2011) 468–480

Contents lists available at ScienceDirect

Journal of Structural Geology

journal homepage: www.elsevier.com/locate/jsg

The interaction of migrating grain boundaries and fluid inclusions in naturally deformed quartz: A case study of a folded and partly recrystallized quartz vein from the Hunsrück Slate, Germany

Joyce Schmatz*, Janos L. Urai

Structural Geology, Tectonics and Geomechanics, RWTH Aachen University, Lochnerstrasse 4-20, 52056 Aachen, Germany

ARTICLE INFO

Article history:
Received 23 August 2010
Received in revised form
2 December 2010
Accepted 21 December 2010
Available online 29 December 2010

Keywords:
Fluid-rock interaction
Hunsrück slate
Multiphase fluid inclusions
Quartz recrystallization, grain boundary morphology

ABSTRACT

We studied the microstructure of a folded and partly recrystallized quartz vein from the Hunsrück Slates in Germany, focusing on the morphology and distribution of fluid inclusions in the old and new grains and along the different types of grain boundaries. Blocky vein quartz grains show undulose extinction and develop subgrains. New grains form by subgrain rotation and grain boundary migration, with a bimodal size distribution.

The old, deformed grains contain numerous, complex, H_2O–CO_2–graphite inclusions, with significant differences in fluid inclusion setting along subgrain boundaries. The new grains have a lower content of H_2O-rich inclusions than the old grains and do not contain graphite, and there is a significant difference in volume and density of fluid inclusions between the large and small new grains. Grain boundaries between old and new grains are irregular, containing similar fluid inclusions as the old grains, but no enrichment in graphite, while grain boundaries between new grains are smooth and can be inclusion-free or contain arrays of fluid inclusions.

We interpret these structures to have formed by a series of complex interactions between grain boundaries migrating at different velocity and the fluid inclusions. Differences in mobility and grain boundary velocity can result in different variations of drag and drop- interaction, while chemical differences lead to phase separation during grain boundary–fluid interaction. Migration of grain boundaries into the old grains was accompanied by significant redistribution of fluids and graphite along the grain boundary together with oxidation of graphitic inclusions to CO_2.

1. Introduction

1.1. Fluid inclusions in recrystallized quartz

Diagenesis and metamorphism involves recrystallization and/or crystal growth. Fluid inclusions entrapped in this process are used as valuable proxies for the nature, composition and density of the fluids present and the temperature and pressure at the time of entrapment (e.g., Roedder, 1984; Muchez et al., 1995). During recrystallization and grain growth, syn- or post-deformational formation and migration of subgrain boundaries is followed by the formation and migration of high angle grain boundaries. The role of fluid inclusions in this processes has been studied in numerous laboratory and field studies and it has been shown that not only the composition of fluid inclusions may change during recovery or recrystallization but also that the recrystallized grain size and grain boundary structure may be affected by the fluid phase (e.g., Tullis and Yund, 1982; Olgaard and Evans, 1986; Schmatz and Urai, 2010).

Primary fluid inclusion arrays that formed during crystal growth from a free solution are typically reworked during the first phase of recrystallization, so that recrystallized grains contain fewer fluid inclusions (e.g., Kerrich, 1976; Roedder, 1984; Drury and Urai, 1990; Mullis et al., 1994; Schléder and Urai, 2007), but to date this process has not been studied in detail.

Additional processes are preferential leakage of fluid inclusions after crystal plastic deformation (e.g., Kerrich, 1976; Wilkins and Barkas, 1978; Hollister, 1990; Vityk et al., 2000; Tarantola et al., 2010). For example, diffusion along dislocations or dislocation networks connecting an inclusion to a grain boundary, can lead to preferential leakage of H_2O from mixed inclusions containing CO_2 and H_2O (Hollister, 1990; Bakker, 1992; Hall and Sterner, 1993). Kerrich (1976) showed that even a small degree of intracrystalline strain might cause leakage from inclusions, resulting in anomalously high homogenization temperatures (Roedder, 1984). However, the

* Corresponding author.
E-mail address: j.schmatz@ged.rwth-aachen.de (J. Schmatz).

0191-8141/$ – see front matter © 2010 Elsevier Ltd. All rights reserved.
doi:10.1016/j.jsg.2010.12.010

movement of inclusions attached to dislocations moving under stress (e.g., Barnes and Mazey, 1963; Roedder, 1971; Wilkins and Barkas, 1978) is not well understood. It has also been demonstrated that fluid inclusions can move along a temperature gradient (Anthony and Cline, 1971).

The morphology of grain boundary fluids is controlled by the ratio of grain boundary energy to the solid–fluid interfacial energy, which also controls the morphology of fluid inclusions along grain boundary triple junctions (Watson and Brenan, 1987). A number of studies describe the grain scale distribution of fluids with respect to the microstructural evolution using samples broken along grain boundaries (e.g., Watson and Brenan, 1987; Olgaard and Fitz Gerald, 1993; Mancktelow et al., 1998; Mancktelow and Pennacchioni, 2004; Schenk et al., 2005). Mancktelow and Pennacchioni (2004) have shown that in dry quartzite mylonites, grain boundaries are smooth and inclusion-free, while wet mylonites contain grain boundary fluid inclusion arrays, presumably filled with metamorphic fluid. Channel structures along these grain boundaries are usually interpreted as dynamic features while development of isolated pores points to more equilibrated stages (Urai, 1983). However, fluid inclusion arrays along grain boundaries can also exist in migrating grain boundaries (as shown for calcite by Schenk et al., 2005).

For the H_2O–CO_2 system, Drury and Urai (1990) proposed that H_2O-rich fluids form continuous fluid films on moving high angle grain boundaries, whereas CO_2-rich fluids do not, based on

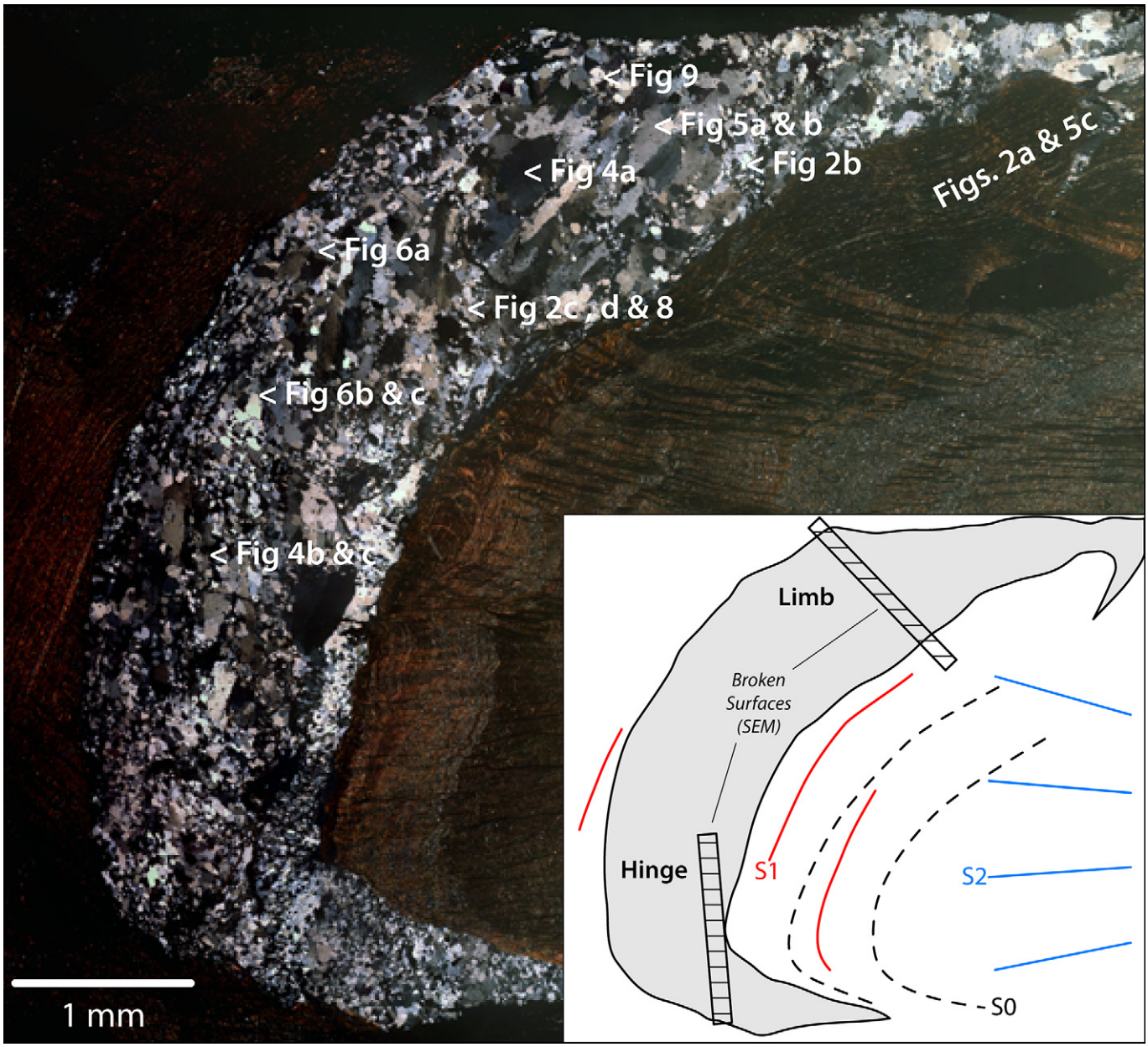

Fig. 1. Micrograph showing folded and partly recrystallized quartz vein from the Hunsrück slate (crossed polarized light, section thickness is 25 μm). Number and size of primary grains decreases from limb to hinge. The recrystallized grain size is bimodal with the majority of large recrystallized (LR) grains in the limb and smaller recrystallized (SR) grains in the hinge. The approximate location of subsequent figures/micrographs is indicated. Note that all micrographs were taken from this section or sections parallel to this one, i.e., perpendicular to the fold axis. Inset: Lines indicate approximate orientation of bedding (S_0), D_1-cleavage (S_1) and D_2-cleavage (S_2). Hatched boxes indicate location of broken surfaces used to study grain boundary morphology (Fig. 9).

observations in natural rocks. They suggested that a moving grain boundary might significantly change the fluid inclusion composition when CO_2 is separated from H_2O being in contact with the boundary. The large difference in wetting characteristics of CO_2 and brines implies that the CO_2-rich fluid would collect at grain boundaries while H_2O is redistributed laterally. With ongoing grain boundary migration involving drag and drop CO_2 might be entrapped inside grains (e.g., Watson and Brenan, 1987; Hollister, 1990; Holness, 1993; Petrishcheva and Renner, 2005; Schmatz et al., in press). Rutter and Brodie (2004) show that the incorporation of water from grain boundaries to the lattice during grain growth contributes to weakening. In addition, hydrocarbons give valuable insights into the recrystallization behavior of minerals, as the fluid phase may contain highly volatile components such as CH_4, but also immobile components such as solid bitumen (Schoenherr et al., 2007) or graphite (Satish-Kumar, 2005). It is well known that a hydrocarbon-bearing second phase affects or can inhibit quartz cementation when hydrocarbons accumulate as coatings in pores (e.g., Aase and Walderhaug, 2005). However, the effect of hydrocarbons during grain boundary migration is not well understood and can be complex (Krabbendam et al., 2003; Schoenherr et al., 2010). Hydrocarbon migration is usually associated with intergranular pores and microfractures (Baron et al., 2008). Only a few workers have discussed the effect of mobile grain boundaries on intracrystalline leakage, phase separation and chemical reactions, which affect maturity diagnostics (e.g., Jensensuis and Burruss, 1990; Buckley et al., 1998; Rantisch et al., 1999).

Drury and Urai (1990) propose that grain boundary migration recrystallization is responsible for eliminating a considerable amount of fluid volume from grains. The process is agreed to be common in metamorphic rocks (e.g., Wilkins and Barkas, 1978), however, there is no detailed understanding on the interaction of moving grain boundaries with fluid inclusions, e.g., of the effect of the magnitude of velocity of the boundary or of fluid inclusion mobility. It is likely that highly mobile fluid inclusions are dragged and redistributed or removed while fluid phases with a low mobility are not affected interacting with a moving grain boundary (Schmatz et al., in press). Also the scale of observation may influence interpretations as there is some evidence that large fluid inclusions tend to breakup into arrays of smaller inclusions which might just not be visible using standard optical microscopy, however, the fluid volume does not necessarily change in this process (Roedder, 1984; Schmatz and Urai, 2010).

1.2. Grain boundary–fluid inclusion interaction in experiment

Experiments on rocks under high pressure and temperature allow control of fluid composition and fugacity, the measurement of stress and strain and subsequent investigation of the microstructure (e.g., Tullis and Yund, 1982; Spiers et al., 1986; Watanabe and Peach, 2002). Analogue experiments using transparent, polycrystalline model materials (salts or organic rock analogues) deformed in transmitted light allow in-situ observation of the microstructural evolution and quantification of the kinetics of migrating grain boundaries and fluid inclusions. For example, the morphology and interconnectivity of fluid films under equilibrium and disequilibrium conditions shows how equilibrium fluid pockets along grain boundaries and grain triple junctions evolve to interconnected fluid films under dynamic conditions and vice versa (Bauer et al., 2000; Schenk and Urai, 2005; Walte et al., 2005).

Experimental models show that leakage and redistribution of fluid inclusions by migrating grain boundaries is usually accompanied by morphology and volume changes of intra- and intercrystalline fluid inclusions. During drag and drop, fluid inclusions can be observed to deform or to neck down (Urai, 1983; Olgaard and Fitz Gerald, 1993; Schmatz and Urai, 2010) or, with appropriate wetting properties, to become fully incorporated into migrating grain boundaries (Schenk and Urai, 2005; Schmatz et al., in press). Other authors (e.g., Brodhag and Herwegh, 2009) have investigated the effects of immobile second phases and their interaction with migrating grain boundaries, which dramatically affects the recrystallized texture.

This paper describes the microstructures formed during recrystallization of a quartz vein containing numerous primary multiphase fluid inclusions. The aim is to better understand the interplay of fluid inclusions and migrating grain boundaries and the resulting effects on grain boundary structure and the recrystallized microstructure.

2. Sample description and geological setting

The sample (Fig. 1) is a naturally deformed quartz vein hosted by slate of the Hunsrück area, Germany. It is the same sample in which Drury and Urai (1990, Fig. 7) first described the redistribution of fluid inclusions in quartz by deformation and recrystallization. Wagner and Cook (2000, and authors therein) and Wagner et al. (2010) give a detailed overview of the Hunsrück regional geology, the formation of the different sets of veins and the formation and alteration of fluid inclusions.

The vein is sub-parallel to bedding and at shallow angle to the regional S_1 cleavage formed during D_1-folding (Hoeppner, 1960; Weber, 1960), and was deformed in the core of a small D_2 fold. A number of splays of the vein cut through the S_1 cleavage and have chlorite-quartz fill growing epitaxially on S_1 (Fig. 1 inset, Fig. S1). The vein is about 2 mm thick, consisting of elongate-blocky (Wagner et al., 2010), milky quartz grains with abundant fluid inclusions and smaller, recrystallized quartz grains which contain fewer and different types of fluid inclusions (Drury and Urai, 1990).

Table 1
Nomenclature.

Abbreviation		Description
Grains		
P	Primary grains	Large, blocky grains with deformation lamellae and appending subgrains. ~16 vol.% fluid content, multiphase fluid inclusions with graphite, ∅ up to 17 μm.
SR	Small recrystallized grains	Equilibrated grains with mean size of 113 μm. ~9.5 vol.% fluid content, transparent single phase inclusions, ∅ up to 14 μm
LR	Large recrystallized grains	Equilibrated grains with mean size of 259 μm. ~5.5 vol.% fluid content, single phase inclusions, ∅ up to 6 μm.
Grain boundaries		
P–P	Adjacent primary grains	Dense serration, fluid-poor, often rotated bulges.
P–LR	Primary grains with large recrystallized grains	Often straight, fluid-poor, sometimes incorporation of graphite, sometimes pinning.
P–SR	Primary grains with small recrystallized grains	Compare with P–LR
SR–SR	Adjacent small recrystallized grains	Commonly straight, fluid-rich, worm-like fluid inclusion morphology.
LR–LR	Adjacent large recrystallized grains	Commonly straight to gently curved, fluid poor, sometimes single-phase graphite inclusion arrays.
SR–LR	Small recrystallized grains with large recrystallized grains	Rare, commonly straight to gently curved. Compare to SR–SR.

Drury and Urai (1990) describe the fluid content to be markedly fewer within new grains compared with primary grains. In this study we carried out a much more detailed analysis to test to what extent the fluid volume is changed with respect to the microstructural processes.

3. Analytical techniques

Samples were cut perpendicular to the fold axis. Double polished thin sections of 25 and 40 μm thickness were used to study fluid inclusion morphology and the vein microstructure in transmitted light polarized microscopy. In addition, we studied the porosity on polished surfaces of the thin sections, sputter-coated with carbon, in SEM (secondary electron mode); post-processed using automated image analysis (Image SXM 18.9). The advantage of this procedure is that the sections are truly 2D (Underwood, 1970; Desbois et al., 2008), and further information on fluid inclusion type and morphology can be derived from the same section by optical microscopy. The results were compared to a number of ultra-high-precision polished surfaces in BIB (Broad Ion Beam)-SEM to quantify the error caused by polishing defects (see Appendix). Parallel reflected light and UV-light microscopy were used to identify the carbonic phase using a photometer equipped with a pinhole aperture to read a spot with a diameter of 5 μm on the sample surface at a wavelength of 546 nm, using a 40×/0.85 lens in oil immersion ($n_e = 1.518$).

We used broken surfaces to study the grain boundary morphology (e.g., Mancktelow et al., 1998). For this purpose we cut the sample in thin slabs, which were broken in two directions: parallel to the D_2-cleavage on the fold limb and perpendicular to the D_2-cleavage and parallel to the D_2 fold axis (Fig. 1). Most fracture surfaces formed along grain boundaries, as demonstrated earlier by e.g., Mancktelow et al. (1998). Samples were sputter-coated with gold and imaged in SEM–SE mode with acceleration voltages of around 15 kV.

4. Observations

4.1. Microstructure

The gently curved limb of the folded quartz vein has two components: large, deformed grains and strain-free recrystallized grains, in approximately equal proportions. Where the degree of recrystallization is low, the old grains show the typical elongate-blocky shape of vein quartz, typical of the veins in nearly all outcrops not deformed by D_2 folds. The other part of the fold is the

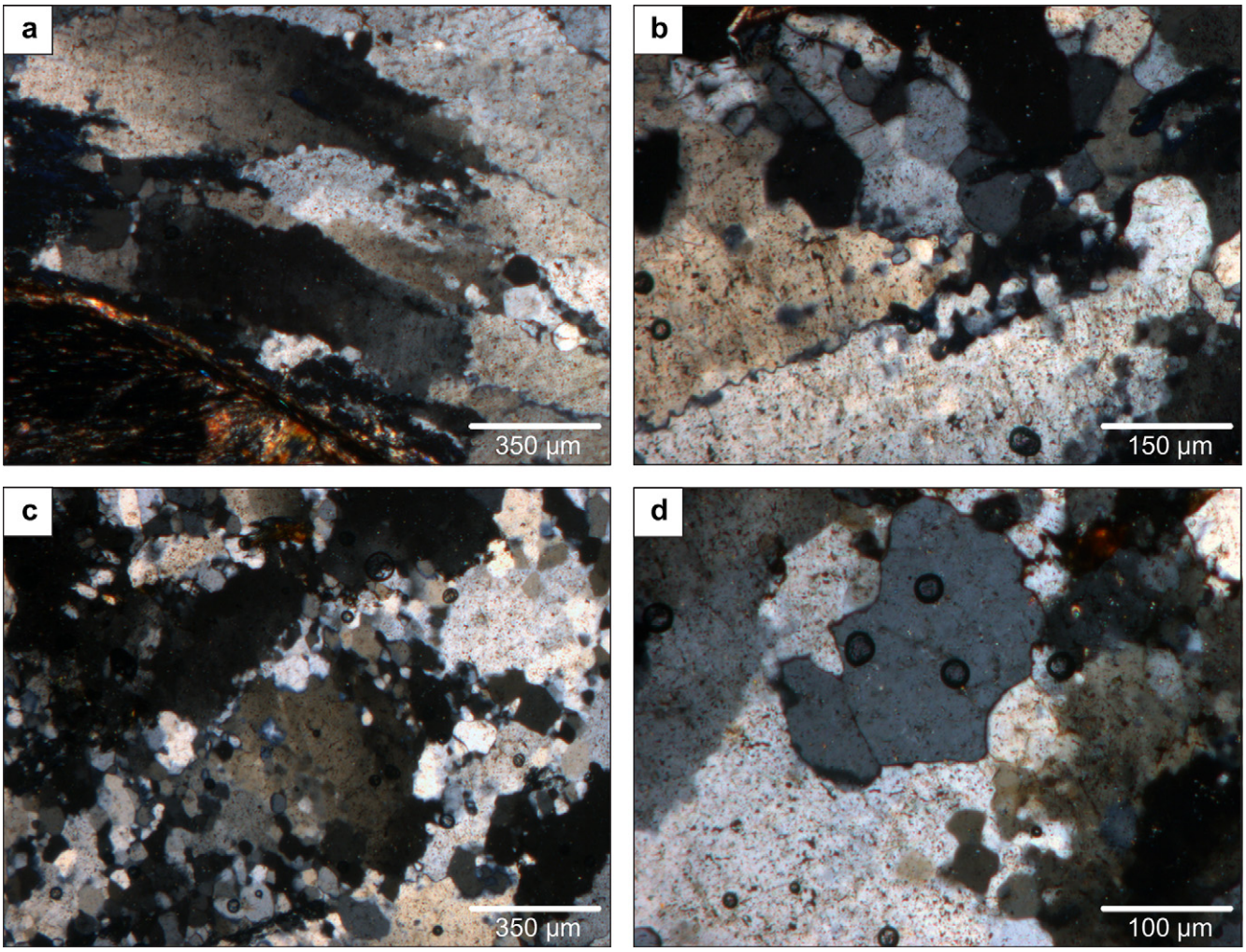

Fig. 2. Micrographs showing (a) elongated primary grains with undulose extinction and serrated grain boundaries, (b) bulging recrystallization and recrystallized grains located at triple junction of primary grains, (c) primary grains mantled by SR- and LR-grains, and (d) LR-grain grown into a primary grain by grain boundary migration recrystallization. Note that dark-rimmed, spherical inclusions are preparation artifacts (crossed polarized light, thin section thickness is 25 μm).

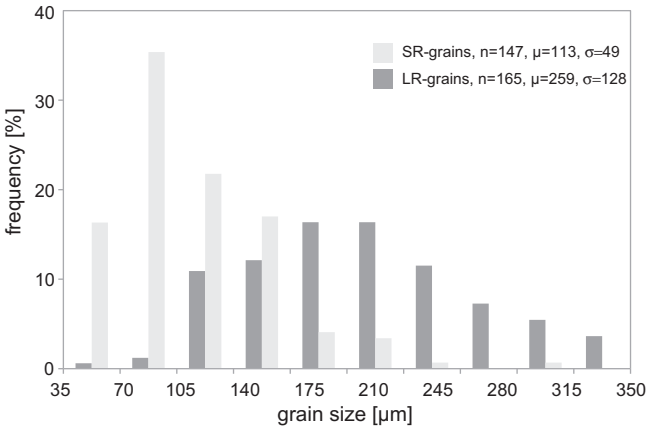

Fig. 3. Grain size histograms showing bimodal size distribution of recrystallized grains. Inclusion-rich recrystallized grains are smaller with a mean grain size of $\mu = 113$ μm (median $\mu+ = 103$, standard deviation $\sigma = 49$, number $n = 147$). Inclusion-poor grains are larger with a mean grain size of $\mu = 259$ μm ($\mu+ = 225$, $\sigma = 128$, $n = 165$).

approximately 1.5 mm thick hinge zone which is almost completely recrystallized (Fig. 1).

In the following we will use the term "primary" (P) for the large, fluid-inclusion-rich, vein-quartz grains (according to Table 1). Within the entire vein inclusion-rich primary grains as well as recrystallized grains are present, which contain less fluid inclusions and tend to be larger on the limb of the fold. Primary grains show evidence for intracrystalline strain with undulose extinction and formation of subgrains; these tend to have a preferred shape orientation at an angle to both S_1 and S_2-cleavage (Fig. 2a, Fig. S2). Grain boundaries between two primary grains are serrated, with bulges of a few micrometers in diameter. New grains, with a crystallographic orientation related to the host grain, are frequently located in the bulges (Fig. 2b; rotated bulges: Stipp and Kunze, 2008) and more abundant at triple junctions of primary grains. Grain boundaries between recrystallized grains are commonly gently curved and meet at 120° angle in triple junctions (Fig. 2c and d, Fig. S3). A few, large, recrystallized grains growing into primary grains tend to have lobate boundaries.

The size distribution of the equilibrated recrystallized grains is bimodal (Fig. 3). Inclusion-rich recrystallized grains are smaller with a mean grain size of $\mu = 113$ μm (median $\mu+ = 103$, standard deviation $\sigma = 49$, number $n = 147$). Inclusion-poor grains are larger with a mean grain size of $\mu = 259$ μm ($\mu+ = 225$, $\sigma = 128$, $n = 165$). Inclusion-rich, smaller recrystallized grains (SR-grains, Table 1) are more abundant but occupy about the same area as inclusion-poor, larger recrystallized grains (LR-grains, Table 1, see full description and discussion of these two kinds of recrystallized grains below).

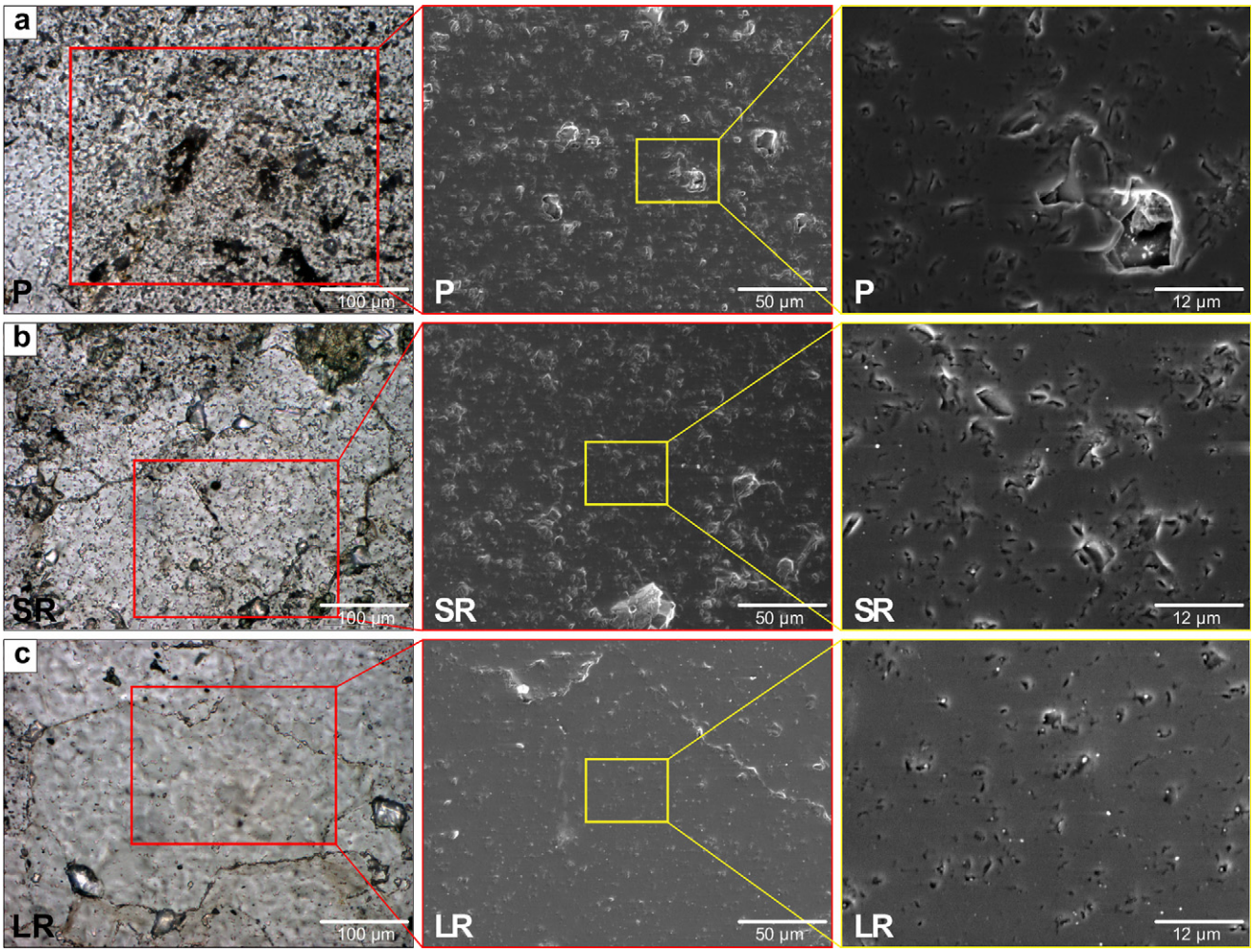

Fig. 4. Micrographs (first column, parallel polarized light, section thickness is 25 μm) and SEM–SE images (second and third column) showing porosity on highly polished section surfaces for (a) Primary grains, (b) SR-grains, (c) and LR-grains. Image analysis was undertaken on rectangular cells with sizes 40 × 40 μm and 120 × 120 μm cut from SEM–SE images (see Appendix for details).

For clarity, the description of fluid inclusions is subdivided into two parts: those within grains and those along grain boundaries. We note that in this paper we only present results on the morphology and distribution of fluid inclusions; results on composition and closure temperature will be presented in a follow-up paper. In this paper we adopt the nomenclature given in Table 1.

4.2. Fluid inclusions in grains

Numerous types of fluid inclusions were observed, ranging from transparent single-phase inclusions to multiphase inclusions containing graphite (bitumen reflection > 8%). The most apparent observation is that the primary grains contain numerous multi-phase inclusions while in the recrystallized grains fluid inclusions less and mainly non-graphitic single-phase inclusions are abundant. In the recrystallized grains two subtypes can be distinguished optically, with one group having less fluid inclusions than the other.

4.2.1. Fluid inclusions in primary grains

The fluid inclusion size and distribution can be estimated from the porosity determined from SEM–SE images of highly polished thin section surfaces (Fig. 4, see the Appendix for a short discussion). Fluid inclusion size and distribution was measured within 14 rectangular cells of 120 × 120 μm taken randomly from 5 different primary grains (N.B. 14 cells from 14 SR-grains and 14 cells from 7 LR-grains, respectively).

Primary grains have a fluid inclusion content of 16 (±2) vol.% of which around 80% is non-graphitic (Fig. 5). In general we find patchy, randomly distributed multiphase fluid inclusions (liquid, vapor, graphite) with sizes up to 18 μm (Fig. 5b). Only a few single-phase inclusions are arranged in arrays associated with micro-cracks. Between the patchy multiphase inclusions we commonly find small (<10 μm), spherical and homogeneously sized single-phase inclusions.

Almost all primary grains show intracrystalline plastic strain (undulose extinction, deformation lamellae) and often the large, patchy, multiphase fluid inclusions occur along subgrain boundaries and on subgrain triple junctions (Fig. 5c). Single-phase inclusions inside subgrains are less frequent compared to parts of the grains, which do not contain subgrains and have straight extinction. Numerous graphite-containing inclusions (Fig. 6 and Fig. S4) were identified inside primary grains and along some grain boundaries of the equilibrated recrystallized grains. Graphite is non-fluorescent but shows high reflectance in white light (>8%, Koch, 1997). The spatial distribution of graphite bearing inclusions in subgrain-free parts of primary grains (Fig. 5) is random and usually these inclusions are composed of at least three phases (liquid, vapor, graphite, and often a non-carbonic solid phase).

4.2.2. Fluid inclusions in recrystallized grains

SR-grains are optically fluid inclusion-rich, and have a fluid fraction of 9.5 (±2) vol.% (Figs. 7 and 8). They contain numerous, single phase inclusions, with sizes up to 14 μm. They are spherical in shape and are homogeneously distributed in the grains. LR-grains are optically fluid-poor grains but contain numerous arrays of single-phase inclusions with sizes up to 6 μm with a fluid fraction of 5.5 (±1) vol.% (Figs. 7 and 8).

4.2.3. Statistics of fluid inclusions in primary and recrystallized grains

All samples have a negative exponential size distribution of inclusions with a similar frequency in primary grains ($\mu = 1.88$, $\mu+ = 1.44$) and small recrystallized grains ($\mu = 1.89$, $\mu+ = 1.31$) with pore sizes up to 18 μm in primary grains up to 14 μm in SR-grains.

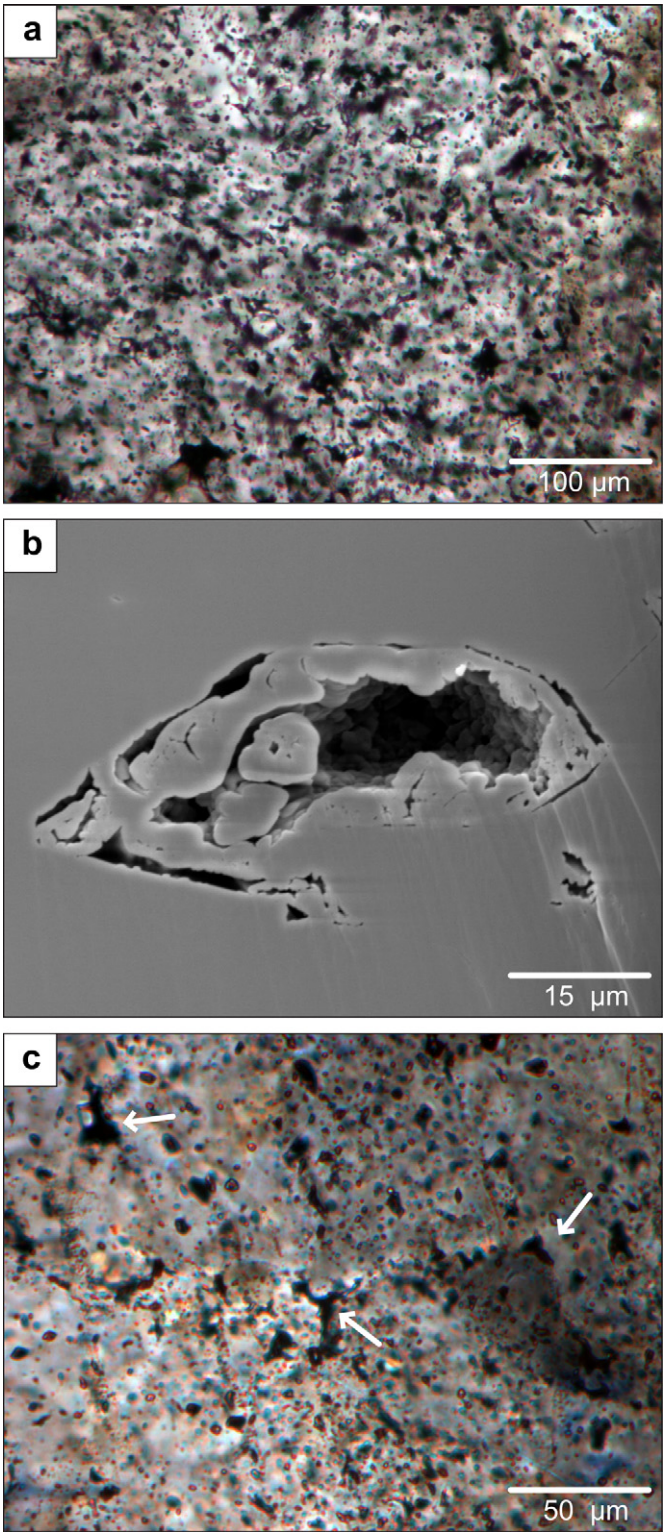

Fig. 5. Micrographs showing (a) multi-phase inclusions (liquid, vapor, graphite) in undeformed Primary grains with interbedded single phase fluid inclusions, (b) a SEM–SE image of a multiphase inclusion cross-cut with BIB and (c) multiphase inclusions in subgrains walls of Primary grains (a and c: partly polarized light, section thickness is 25 μm).

LR-grains ($\mu = 1.32$, $\mu+ = 1.02$) do not contain pores larger than 6 μm (Fig. 7a).

Homogeneous spatial distribution was tested and validated with *t*-statistics (confidence interval is 95%) on the number (count) of

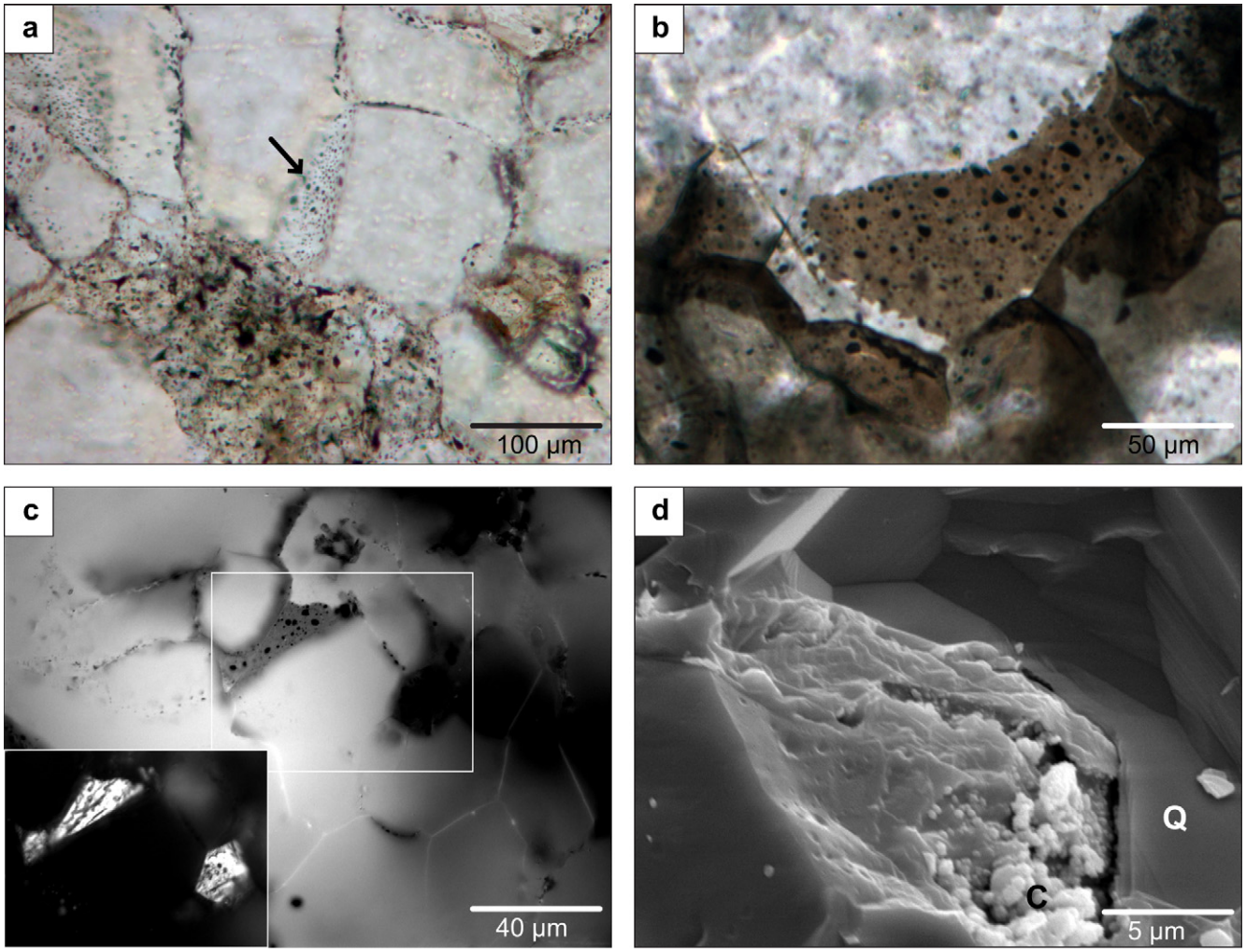

Fig. 6. Graphite inclusions and graphitic grain boundary coating in Primary grains (a) and along grain boundaries of LR-grains (a–d). (a) and (b) are parallel polarized micrographs from a 40 µm thick section, (c) is the same section in UV-light (inset: reflected light) and (d) shows graphite coating (C) on a grain boundary in SEM–SE mode.

fluid inclusions of individual size classes (Fig. 7b). Additionally it was shown that all samples have a comparable number of fluid inclusions in the size class of 4–5.99 µm.

To test the similarity of the three grain-types the Mann–Withney *U*-test was performed (e.g., Sachs, 2004). For the fluid inclusion size range of 1–20 µm (Fig. 7) primary grains and SR-grains have a similar distribution ($z = 0.45$, significance level is 5%) and also the distribution of fluid inclusions in SR- and LR-grains is similar ($z = 1.13$). Primary grains and LR-grains are non-similar ($z = 1.66$) with respect to the fluid inclusion distribution. The same test was performed for small size classes (0–5.99 µm). All samples within this size range were similar to each other (P-grains vs. SR-grains: $z = 0.38$, P-grains vs. LR-grains: $z = 1.29$, and SR-grains vs. LR-grains: $z = 0.68$).

4.3. Fluid inclusions in grain boundaries

Six different types of grain boundaries were observed at contacts of (i) adjacent primary grains (P–P), (ii) primary grains with fluid-poor LR-grains (P–LR), (iii) primary grains with fluid-rich SR-grains (P–SR), (iv) adjacent fluid-rich SR-grains (SR–SR), (v) adjacent fluid-poor LR-grains (LR–LR), (vi) fluid-rich SR-grains with fluid-poor LR-grains (SR–LR) (Figs. 8 and 9, Table 1).

Adjacent primary grains in direct contact but without rotated bulges (Fig. 9a) show a dense serration and are relatively fluid inclusion-poor. Grain boundaries of rotated bulges with primary grains are comparable to P–LR boundaries (see below, Fig. 9b).

Grain boundaries of primary grains with SR- or LR-grains, respectively, do not show major differences. In optical micrographs these boundaries appear as a clear separation of inclusion-rich primary grains and recrystallized grains. An accumulation of fluids or graphite along grain boundaries is not observed. SEM observations show serrated boundaries of primary grains being in contact with smooth grain boundaries of recrystallized grains with local increase in grain boundary porosity (Fig. 9c). In some cases we observe that the aqueous or gaseous phase separates from the graphitic phase while being in contact with a grain boundary. Here two opposing processes can be distinguished: (i) the aqueous/gaseous phase is incorporated into the grain boundary and the graphitic phase is left behind in the bulk grain (Fig. 10a) and (ii) the graphitic phase is incorporated into a grain boundary leaving behind the aqueous/gaseous phase as inclusions in the bulk grain (Fig. 10b) The preserved fluid inclusion morphology suggested that a necking process caused separation (Fig. 10a and b). Well-equilibrated inclusion arrays along grain boundaries show the ability to pin grain boundaries (Fig. 10c). Carbonic inclusions inside recrystallized grains are rare.

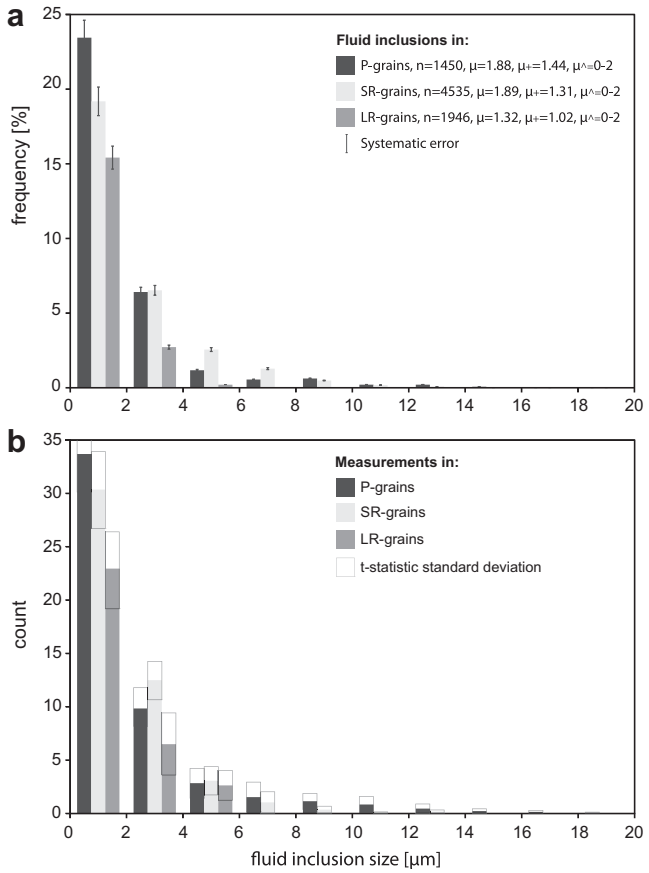

Fig. 7. Histograms showing (a) fluid inclusion size frequency as derived from SEM–SE images (μ = mean, μ+ = median, μ^ = modal) with a bin size of 2 μm and (b) the number of fluid inclusions measured in rectangular cells of 120 × 120 μm with a bin size of 2 μm. For each grain type (P, SR and LR, Table 1) we analyzed 14 cells taken randomly from 5 to 7 grains. T-statistics points to a homogeneous distribution of fluid inclusions. The fluid fraction is 16 vol.% in primary grains, 9.5 vol.% in SR-grains and 5.5 vol.% in LR-grains. See text for more information.

Single-phase fluid inclusions along grain boundaries of SR-grains show a distinct morphology. They have a worm-like morphology and build a dense network with a ridge-channel structure. In micrographs the network appears to have a high connectivity, which is supported by SEM–SE images (Figs. 8 and 9d).

Grain boundaries of adjacent LR-grains show only few fluid inclusions, and these are well-equilibrated. Also, some grain boundaries of this type contain graphite (Figs. 6 and S4). SEM–SE imaging shows that fluid inclusions along grain boundaries of LR-grains are isolated, well-equilibrated arrays of inclusions which often adopt a negative crystal shape. The inclusions are small (usually < 1 μm). Size and distribution may vary from grain boundary to grain boundary and also two or more size classes may occur on a single grain boundary (Fig. 9e). The suggestion that depressions in the grain boundary surface are opposed by depressions on the other side of the grain boundary (Olgaard and Fitz Gerald, 1993) is confirmed by SEM observation of BIB-polished faces (Fig. 9f). Graphite inclusions at LR–LR boundaries are single phase with sizes ranging from 0.3 to 7.5 μm (Fig. 11), usually arranged in arrays. In most cases graphitic inclusions are well-equilibrated to spheres and evenly distributed. In the vicinity of primary grains LR–LR boundaries are sometimes coated with a transparent brownish film which can also be identified as graphite along broken surfaces in the SEM (Fig. 6d).

Small recrystallized grains and large recrystallized grains usually appear in clusters and these clusters are often separated by primary grains or chlorite bands (Figs. 2 and S2). Accordingly SR–LR boundaries are not frequent. SR–LR boundaries are comparable to the SR–SR boundary structure with numerous single-phase inclusions arranged in a dense network (Fig. 8).

5. Discussion

5.1. Fluid inclusions in primary grains

The orientation of the vein with respect to the bedding and intersection with S_1 cleavage suggests that originally the veins were sub-parallel to bedding but formed after the formation of S_1 cleavage. The conditions of entrapment of hydrocarbon fluid inclusions cannot fully be reconstructed for the present sample. Hydrocarbons are commonly incorporated in cement during diagenesis along intergranular porosity or along cracks (e.g., Baron et al., 2008). In these quartz veins, we interpret the observations to be the result of migration of brines, CO_2 and hydrocarbons, which allowed incorporation of the mixed fluid into authigenic grains before peak temperatures, likely post-D_1 in the Hunsrück Basin, which was later transformed to graphite (Munz et al., 1995; Parnell et al., 1996).

In the primary grains the large, patchy, multiphase fluid inclusions are enriched in subgrain boundaries and in subgrain triple junctions, most likely formed during D_2 deformation (Fig. 5b). Single-phase inclusions inside subgrains are less frequent than in parts of those grains, which do not contain subgrains and have straight extinction. The variable phase ratios in the large fluid inclusions suggest post-entrapment modifications by leakage and associated transport of the mobile phases, for example along mobile dislocations or subgrain boundaries. These observations are consistent with the mobility of subgrain boundaries during subgrain rotation, causing the carbonic inclusions to collect on the subgrain boundaries (Green and Radcliffe, 1975; Wilkins and Barkas, 1978; Vityk et al., 2000). Dislocation climb allows transport of fluid inclusions into subgrain walls accompanied by further leakage and phase separation by necking processes. Bulging recrystallization, also related to D_2, is associated with an elimination of fluid inclusions within the nucleus (Kerrich, 1976).

5.2. Fluid inclusions in recrystallized grains

The majority of recrystallized grains are strain-free and the boundaries between recrystallized grains are equilibrated. This can be interpreted as a static component of recrystallization, and therefore we suggest that these new grains were formed after the end of D_2 deformation, which folded the quartz vein. These D_2 folds in the Hunsrück formed under greenschist metamorphic conditions with peak temperatures being estimated in the range of 350–420 °C and pressures of 2–4 k bar (Oncken et al., 1995; Wagner and Cook, 2000; Wagner et al., 2010).

Measurements of fluid volume fraction in the primary and recrystallized grains (SR and LR) point to differences between all three and the statistics support this significant difference for P- and LR-grains and also for LR-and SR-grains. The main difference between the primary grains and the SR-grains is in the presence of large (more than 10 μ) inclusions in the primary grains, which usually contain graphite and fluid. The difference from the LR-grains is that fluid Inclusions larger than 6 μm are absent. These differences clearly point to a reduction of the abundance of water-rich fluids during recrystallization. Different rates for SR- and LR-grains could be explained by (i) LR-grains formed from relatively perfect cores by nucleation and successive growth (Humphreys,

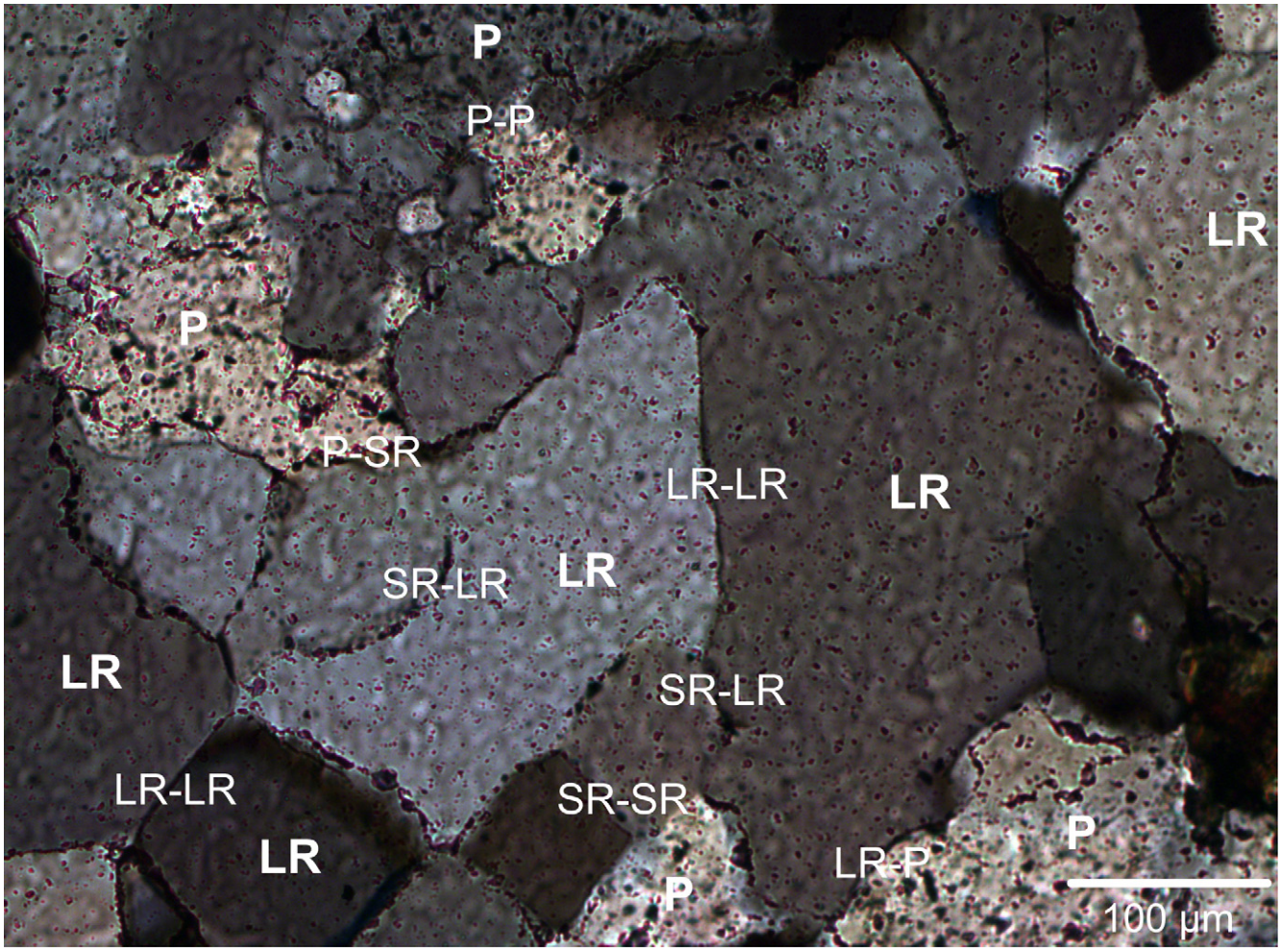

Fig. 8. Micrograph showing primary grains (P), SR-grains and LR-grains (crossed polarized light, section thickness is 25 µm). See Table 1 for explanation of abbreviations and text for a description of grain boundary structures.

2004) and the fluid-enriched SR-grains result from rotation recrystallization preserving most of the primary fluid volume or (ii) this difference in grain size and fluid inclusion content in the two recrystallized grain classes could have been caused by different grain boundary migration velocities leading to differences in the interaction of moving grain boundaries with fluid inclusions (cf. Schmatz and Urai, 2010; Schmatz et al., in press).

We observe that primary grains and SR-grains, especially in the fold hinge, have a similar distribution of fluid inclusion sizes inside bulk grains with respect to the aqueous/gaseous inclusions (large and patchy multiphase inclusions are not found inside recrystallized grains). The detailed analysis of individual size classes in all kinds of grains shows that the recrystallization process has only minimal effect on the distribution of fluid inclusions in a class ranges 0–5.99 µm (Fig. 7c, all samples are statistically similar in this size range). From experiments and models (e.g., Olgaard and Fitz Gerald, 1993; Schenk and Urai, 2005; Schmatz and Urai, 2010) it is well known that drag and drop produces fluid inclusions in recrystallized grains but also that grain boundaries can pass fluid inclusions without interaction, which preserves fluid inclusions in grains. The interaction of grain boundaries and fluid inclusions, which involves drag and drop of fluid inclusions, grain boundary pinning, but also that fluid inclusions are passed by migrating grain boundaries without interaction, is governed by the grain boundary velocity and the fluid inclusion size, e.g., for the same grain boundary velocity a small fluid inclusion is dragged for longer distances than a large one (Schmatz and Urai, 2010; Schmatz et al., in press). The formation of fluid inclusions in the recrystallized grains can be either due to the migrating grain boundary not interacting with a certain class of fluid inclusions (defined by size or composition, Schmatz et al., in press) but moving others, or that all fluid inclusions are moved into a grain boundary fluid phase and form new inclusions by drag and drop processes. Our data do not allow these two processes to be distinguished.

It is often described that recrystallization under lower metamorphic conditions leads to clear, inclusion-free grains (Wilkins and Barkas, 1978; Mullis, 1987; Drury and Urai, 1990). As we observe abundant fluid inclusions also in recrystallized grains we propose that in this first phase of recrystallization, grain boundary migration does not fully eliminate fluid inclusions from grains. We see leakage and a certain amount of fluid redistribution but approximately 50% of the primary fluid volume is preserved. Additional passes by grain boundaries during ongoing dynamic recrystallization are needed to fully clear all inclusions from the grains.

5.3. Fluid inclusions in grain boundaries

In contrast to SR–SR boundaries, there is no obvious accumulation of aqueous single-phase inclusions on P–SR or P–LR

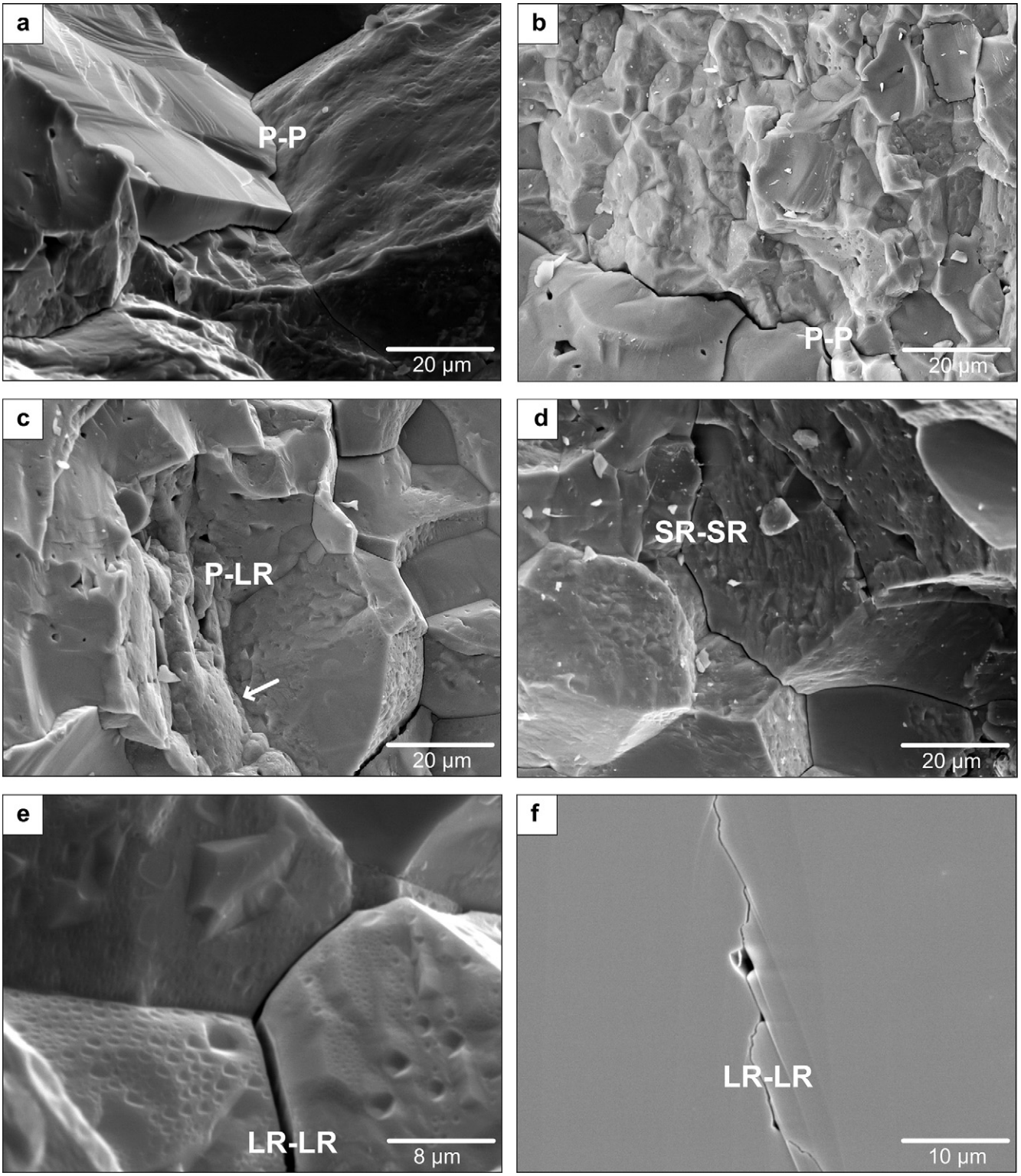

Fig. 9. SEM–SE images on broken surfaces showing (a) a P–P grain boundary, (b) a P–P grain boundary with appending bulges, (c) P–LR grain boundaries, (d) SR–SR grain boundaries, and (e) LR–LR grain boundaries. (f) is an SEM–SE image from a BIB-polished surface showing a cross-cut LR–LR grain boundary.

boundaries although their amount reduces from 13% to 5.5% in large LR-grains compared to primary grains. This points to lateral fluid movement leading to leakage and redistribution of fluids along grain boundaries (e.g., Drury and Urai, 1990; Schléder and Urai, 2007). Schmatz and Urai (2010) give experimental evidence for leakage of fluid inclusions in contact with migrating grain boundaries.

Also, graphitic inclusions do not accumulate at P–SR or P–LR boundaries. Schoenherr et al. (2007) report bituminous fluid inclusions along grain boundaries and inside recrystallized grains in

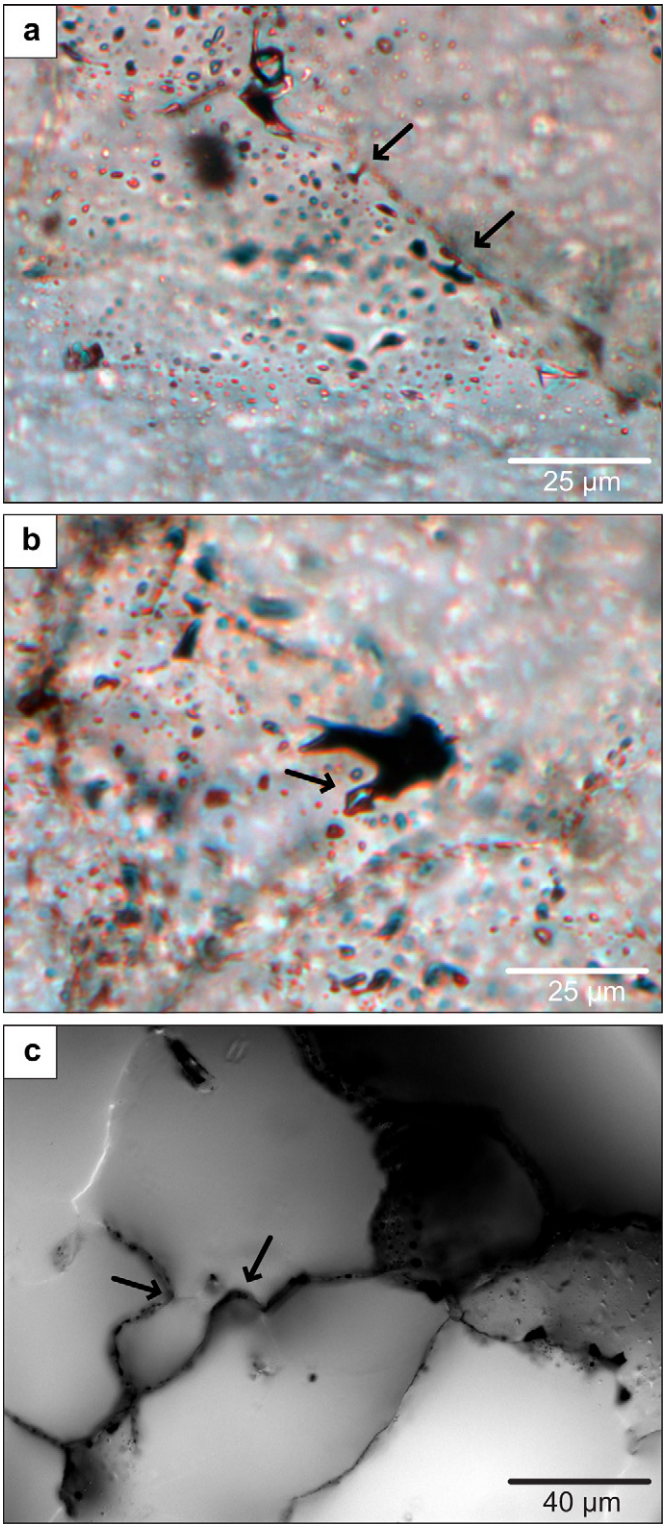

Fig. 10. (a) Micrograph showing morphology of mixed inclusions being in contact with grain boundaries. The aqueous/gaseous phase is incorporated along tubes while the graphitic phase is left behind in the bulk primary grain. (b) Micrograph showing incorporation of the carbon-bearing phase into a grain boundary. In this process the aqueous/gaseous phase separates and is left behind in the bulk grain ((a) and (b): parallel polarized light, section thickness is 40 µm). (c) Micrograph showing well-equilibrated carbonic inclusions along grain boundaries of adjacent recrystallized grains. Highly curved grain boundaries point to pinning effects (UV-light, section thickness is 40 µm).

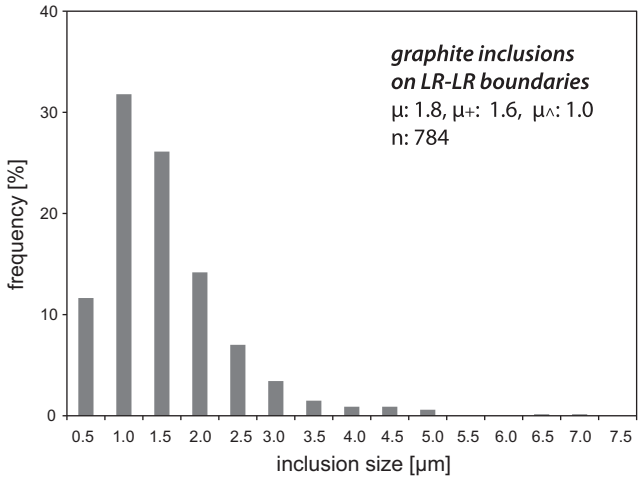

Fig. 11. Histogram showing graphite inclusion size distribution along LR–LR grain boundaries as derived from micrographs (e.g., Fig. 6).

rock salt. They propose that transport of these inclusions by migrating grain boundaries must have been taken place before degradation to solid bitumen. However, such a model does not apply to this quartz sample as recrystallization here requires temperatures >350 °C (e.g., Stipp et al., 2002) that would cause the formation of graphite, which is unlikely to be transported by migrating grain boundaries in the present proportions (Figs. 6 and 10).

Temperatures >350 °C enhance oxidation of graphite to CO and CO_2 in the presence of O_2, H_2O and CO_2 (e.g., Kreulen et al., 1980; Zheng et al., 1996). Contacts to grain boundaries bearing such fluids would enable graphite transformation to CO_2 which can be transported along the grain boundary to form new inclusions.

In LR–LR boundaries, in the vicinity of primary grains, we sometimes observe arrays of single-phase graphitic inclusions and graphitic coatings (Figs. 6 and S4). On the other hand, graphite is never observed on SR–SR grain boundaries (Fig. 8). We interpret these observations to be related to partial oxidation of graphite during recrystallization, while part of the graphite is redistributed along new grain boundaries. Due to their low mobility graphitic inclusions are not further dragged or dropped (Schmatz et al., in press), but instead tend to pin a grain boundary (Fig. 10c).

Also in contrast to SR–SR boundaries, grain boundaries of adjacent LR-grains contain few fluid inclusions. It has been shown in earlier studies (e.g., Drury and Urai, 1990; Schenk and Urai, 2005; Schleder and Urai, 2007) that grain boundary migration induces changes in fluid distribution and volume in grains. In our case, the reason for the difference may be due to the velocity of edge-wise propagation of grain boundaries, e.g., when two newly formed grains are consuming an old grain, their boundary is also extended, but more work is needed to explain this difference.

Next to abundant fluid inclusions inside SR-grains we observe a network of numerous fluid inclusions and fluid inclusion channels along their grain boundaries. The enrichment of transparent single-phase grain boundary fluids in these grains is interpreted being related to the oxidation of graphite to CO_2. Necking down of grain boundary fluid films subsequent to grain boundary migration then causes further breakup into channel structures or isolated inclusions. The high accumulation of CO_2-inclusions formed in these processes could also contribute to pinning effects and preserve the small grain size (Drury and Urai, 1990; Johnson and Hollister, 1995; Brodhag and Herwegh, 2009).

On LR–LR boundaries we observe small (<3 µm), well-equilibrated single-phase fluid inclusions arranged in arrays. These

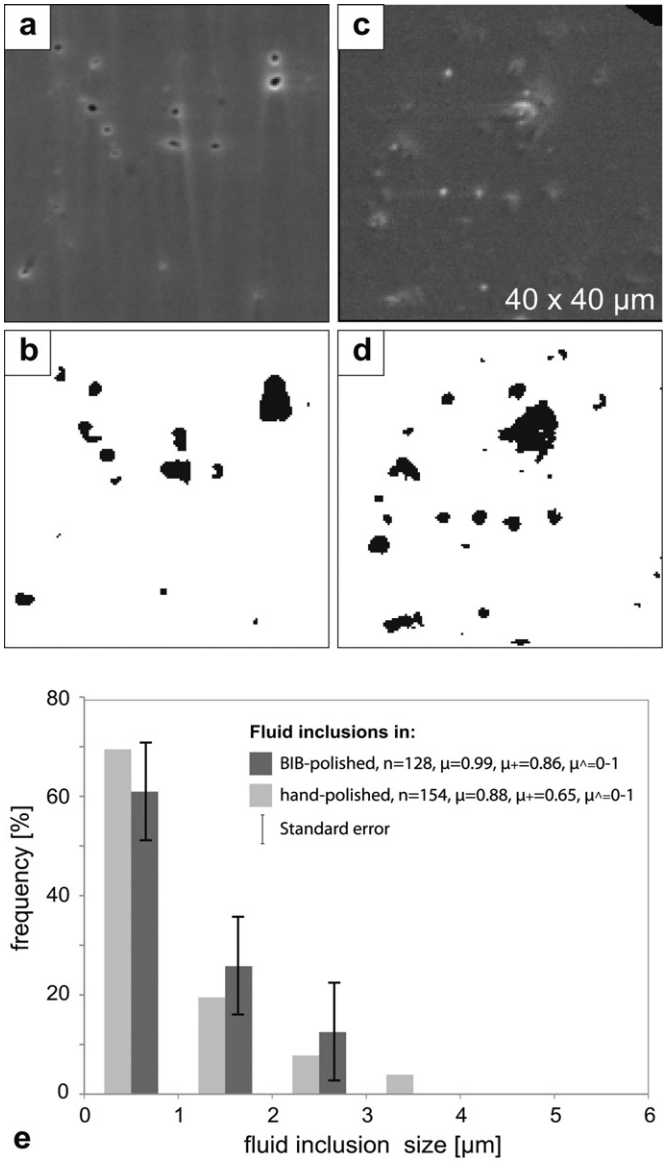

Fig. 12. (Appendix) Figure showing (a) rectangular cell taken from SEM–SE image of an BIB-polished surface of an LR-grain and (b) the same image in binary mode used for image analysis. (c) is a cell taken from SEM–SE image of an manually-polished surface of an LR-grain and (d) the same image in binary mode used for image analysis. The histogram in (e) shows the frequency of fluid inclusion sizes for BIB- and manually polished surfaces for 10 samples each.

arrays are interpreted to have formed from a semi-continuous fluid film present during grain growth which evolved into well-equilibrated inclusions after the grain boundaries stopped moving (Urai et al., 1986; Schenk and Urai, 2005).

6. Conclusions

1. Carbonic inclusions formed from liquid hydrocarbons within the fracture where quartz was growing from hydrothermal fluid, most likely early, with the fractures oriented sub-parallel to bedding. Static recrystallization of the folded quartz occurred after D_2 deformation at 350–420 °C. Hydrocarbons were then converted to graphite under increased temperatures.
2. Deformation and formation of subgrains in primary grains involved interaction of mobile subgrain boundaries with the graphitic inclusions during D_2 deformation.
3. Water-rich fluid inclusions are significantly more abundant in small recrystallized grains than in large grains (9.5 vs. 5.5 vol.%), while primary grains contain approximately 13 vol.% aqueous/gaseous inclusions. These differences point to a reduction of water-rich fluid during recrystallization, at different rates for small and large new grains.
4. Grain boundaries between small recrystallized grains do not contain graphite, while grain boundaries between large recrystallized grains can contain graphite in the vicinity of primary grains.
5. Fluid inclusions in primary grains were not fully removed by a single pass of a grain boundary. It is proposed that removal of fluid inclusions from grains by grain boundary migration occurs by several passes of grain boundary, and different phases are removed at different rates.
6. Grain boundaries between primary and recrystallized grains do not show enrichment of graphite or increasing abundance of fluid inclusions, although these are the locations of the largest transport of these phases out of the primary grains. The migration of grain boundaries into deformed primary grains involves movement of graphite into the grain boundary associated with oxidation to CO_2 and also transport of part of the water-rich phase along the grain boundary. Another part is included into the growing grains by drag and drop processes.

Acknowledgements

We thank W. Kraus, U. Wollenberg and C.M. Diebel for technical assistance. O. Schenk is acknowledged for his comments on an earlier version of the manuscript. The manuscript was significantly improved by thorough reviews by N. Mancktelow and A. Schmidt Mumm. T. Blenkinsop is acknowledged for his editorial help. This research was funded by the German Science Foundation (DFG, UR 64/8-1) and was part of the European Science Foundation (ESF) funded collaborative research Project EuroMinSci.

Appendix

Fluid fraction and spatial distribution of fluid inclusions was measured on manually polished thin section surfaces. BIB (Broad Ion Beam)-polished surfaces (Desbois et al., 2008) give the true 2D-porosity of an infinite small section, which also represents the 3D pore volume (Underwood, 1970). In order to validate our measurements on the manually polished surfaces we compare results with measurements on a BIB-polished surface, both on an LR-grain (Fig. 12). SEM–SE images of grains were subdivided into 10 rectangular cells of 40 × 40 µm. We compare the frequency of fluid inclusion size classes and results show that the deviation is within the standard error (Fig. 12e). The high number of inclusions in the size class 0–1 µm for manually polished samples points to polishing defects.

Appendix. Supplementary data

Supplementary data associated with this article can be found in the on-line version, at doi:10.1016/j.jsg.2010.12.010.

References

Aase, N.E., Walderhaug, O., 2005. The effect of hydrocarbons on quartz cementation: diagenesis in the Upper Jurassic sandstones of the Miller Field, North Sea, revisited. Petroleum Geoscience 11, 215–223.
Anthony, T.R., Cline, H.E., 1971. Thermal migration of liquid droplets through solids. Journal of Applied Physics 42, 3380–3388.
Bakker, R. J., 1992. On modifications of fluid inclusions in quartz. Re-equilibration experiments and thermodynamic calculations on fluids in natural quartz, Ph.D. thesis. Rijksuniversiteit Utrecht.

Barnes, R.S., Mazey, D.J., 1963. The migration and coalescence of inert gas bubbles in metals. Proceedings of the Royal Society of London 275, 47–57.
Baron, M., Parnell, J., Mark, D., Carr, A., Przyjalgowski, M., Feely, M., 2008. Evolution of hydrocarbon migration style in a fractured reservoir deduced from fluid inclusion data, Clair Field, west of Shetland. UK Marine and Petroleum Geology 25, 153–172.
Bauer, P., Palm, S., Handy, M.R., 2000. Strain localization and fluid pathways in mylonite: inferences from in situ deformation of a water-bearing quartz analogue (norcamphor). Tectonophysics 320, 141–165.
Brodhag, S.H., Herwegh, M., 2009. The effect of different second-phase particle regimes on grain growth in two-phase aggregates: insights from in situ rock analogue experiments. Contributions to Mineralogy and Petrology 160, 219–238.
Buckley, J.S., Hirasaki, G.J., Liu, Y., von Drasek, S., Wang, J.-X., Gill, B.S., 1998. Asphaltene precipitation and solvent properties of crude oils. Petroleum Science and Technology 16, 251–285.
Desbois, G., Urai, J.L., Burkhardt, C., Drury, M.R., Hayles, M., 2008. Cryogenic vitrification and 3D serial sectioning using high resolution cryo-FIB SEM technology for brine-filled grain boundaries in halite: first results. Geofluids 8, 60–72.
Drury, M.R., Urai, J.L., 1990. Deformation-related recrystallization processes. Tectonophysics 172, 235–253.
Green, H.W., Radcliffe, S.V., 1975. Fracture at interfaces. Butterworths 1969. In: Grifkins, R.C. (Ed.), Interfaces Conference. Australian Institute of Metals, Melbourne, pp. 223–236.
Hall, D.L., Sterner, M.S., 1993. Preferential water loss from synthetic fluid inclusions. Contributions to Mineralogy and Petrology 114, 489–500.
Hoeppner, R., 1960. Ein Beispiel fur die zeitliche Abfolge tektonischer Bewegungen aus dem Rheinischen Schiefergebirge. Geologie en Mijnbouw 39, 181–188.
Hollister, L.S., 1990. Enrichment of CO_2 in fluid inclusions in quartz by removal of H_20 during crystal-plastic deformation. Journal of Structural Geology 12, 895–901.
Holness, M.B., 1993. Temperature and pressure-dependence of quartz aqueous fluid dihedral angles – the control of adsorbed H_2O on the permeability of quartzites. Earth and Planetary Science Letters 117, 363–377.
Humphreys, F.J., 2004. Nucleation in recrystallization. Materials Science Forum 467–470, 107–116.
Jensensuis, J., Burruss, R.C., 1990. Hydrocarbon–water interactions during brine migration: evidence from the composition of hydrocarbon inclusions in calcite from the Danish North Sea oil fields. Geochimica et Cosmochimica Acta 54, 23–59.
Johnson, E.L., Hollister, L.S., 1995. Syndeformational fluid trapping in quartz – determining the pressure–temperature conditions of deformation from fluid inclusions and the formation of pure CO_2 fluid inclusions during grain-boundary migration. Journal of Metamorphic Geology 13, 239–249.
Kerrich, R., 1976. Some effects of tectonic recrystallisation on fluid inclusions in vein quartz. Contributions to Mineralogy and Petrology 59, 195–202.
Krabbendam, M., Urai, J.L., van Vliet, L.J., 2003. Grain size stabilisation by dispersed graphite in a high-grade quartz mylonite: an example from Naxos (Greece). Journal of Structural Geology 25, 855–866.
Kreulen, R., 1980. CO_2-Rich fluids during regional metamorphism on Naxos (Greece): carbon isotopes and fluid inclusions. American Journal of Science 280, 745–771.
Mancktelow, N.S., Grujic, D., Johnson, E.L., 1998. An SEM study of porosity and grain boundary microstructure in quartz mylonites, Simplon fault zone, Central Alps. Contributions to Mineralogy and Petrology 13, 71–85.
Mancktelow, N.S., Pennacchioni, G., 2004. The influence of grain boundary fluids on the microstructure of quartz-feldspar mylonites. Journal of Structural Geology 26, 47–69.
Muchez, P., Slobodnik, M., Viaene, W.A., Keppens, E., 1995. Geochemical constraints on the origin and migration of palaeofluids at the northern margin of the Variscan foreland, southern Belgium. Sedimentary Geology 96, 191–200.
Mullis, J., 1987. Fluid inclusion studies during very low-grade metamorphism. In: Frey, M. (Ed.), Low Temperature Metamorphism. Blackie, Glasgow, pp. 162–199.
Mullis, J., Dubessy, J., Poty, B., O'Neil, J., 1994. Fluid regimes during late stage of a continental collision: physical, chemical, and stable isotope measurements of fluid inclusions in fissure quartz from a geotraverse through the Central Alps, Switzerland. Geochimica et Cosmochimica Acta 58, 2239–2267.
Munz, I.A., Yardley, B.W.D., Banks, D.A., Wayne, D., 1995. Deep penetration of sedimentary fluids in basement rocks from southern Norway: evidence from hydrocarbon and brine inclusions in quartz veins. Geochimica et Cosmochimica Acta 59, 239–254.
Olgaard, D.L., Evans, B., 1986. Effect of 2nd-phase particles on grain-growth in calcite. Journal of the American Ceramic Society 69, C272–C277.
Olgaard, D.L., Fitz Gerald, J.D., 1993. Evolution of pore microstructures during healing of grain boundaries in synthetic calcite rocks. Contributions to Mineralogy and Petrology 115, 138–154.
Oncken, O., Massone, H.J., Schwab, M., 1995. Metamorphic evolution of the Rhenohercynian zone. In: Dallmeyer, R.D., Franke, W., Weber, K. (Eds.), Pre-permian Geology of Central and Western Europe. Springer, Berlin, Heidelberg, New York, pp. 82–86.
Parnell, J., Carey, P.F., Monson, B., 1996. Fluid inclusion constraints on temperatures of petroleum migration from authigenic quartz in bitumen veins. Chemical Geology 129, 217–226.
Petrishcheva, E., Renner, J., 2005. Two-dimensional analysis of pore drag and drop. Acta Materialia 53, 2793–2803.
Rantisch, G., Jochum, J., Sachsenhofer, R.F., Russegger, B., Schroll, E., Horsfield, B., 1999. Hydrocarbon-bearing fluid inclusions in the Drau range (Eastern Alps, Austria): implications for the genesis of Bleiberg-type Pb-Zn deposits. Mineralogy and Petrology 65, 141–159.
Roedder, E., 1971. Fluid-inclusion evidence on the environment of formation of mineral deposits of the southern Appalachian valley. Economic Geology 66, 777–791.
Roedder, E., 1984. Fluid Inclusions. Mineralogical Society of America.
Rutter, E.H., Brodie, K.H., 2004. Experimental intracrystalline plastic flow in hot-pressed synthetic quartzite prepared from Brazilian quartz crystals. Journal of Structural Geology 26, 259–270.
Sachs, L., 2004. Angewandte Statistik. Springer, Berlin, Heidelberg, New York.
Satish-Kumar, M., 2005. Graphite-bearing CO_2-fluid inclusions in granulites: insights on graphite precipitation and carbon isotope evolution. Geochimica et Cosmochimica Acta 69, 3841–3856.
Schenk, O., Urai, J.L., 2005. The migration of fluid-filled grain boundaries in recrystallizing synthetic bischofite: first results of in-situ high-pressure, high-temperature deformation experiments in transmitted light. Journal of Metamorphic Geology 23 (8), 695–709.
Schenk, O., Urai, J.L., Evans, B., 2005. The effect of water on recrystallization behavior and grain boundary morphology in calcite-observations of natural marble mylonites. Journal of Structural Geology 27, 1856–1872.
Schléder, Z., Urai, J.L., 2007. Deformation and recrystallization mechanisms in mylonitic shear zones in naturally deformed extrusive Eocene-Oligocene rocksalt from Eyvanekey plateau and Garmsar hills (Central Iran). Journal of Structural Geology 29, 241–255.
Schmatz, J., Schenk, O., Urai, J. L. in press. The effect of fluid inclusion-grain boundary interaction on grain boundary migration recrystallization – results from annealing experiments on different rock analogue-pore fluid systems. Contributions to Mineralogy and Petrology. doi:10.1007/s00410-010-0590-3.
Schmatz, J., Urai, J.L., 2010. The interaction of fluid inclusions and migrating grain boundaries in a rock analogue: deformation and annealing of polycrystalline camphor–ethanol mixtures. Journal of Metamorphic Geology 28, 1–18.
Schoenherr, J., Schléder, Z., Urai, J.L., Littke, R., Kukla, P.A., 2010. Deformation mechanisms of deeply buried and surface-piercing late-Precambrian to early-Cambrium Ara salt from interior Oman. International Journal of Earth Sciences 99, 1007–1025.
Schoenherr, J., Urai, L.L., Kukla, P.A., Littke, R., Schleder, Z., Larroque, J.M., Newall, M.J., Al-Abry, N., Al-Siyabi, H.A., Rawahi, Z., 2007. Limits to the sealing capacity of rock salt: a case study of the infra-Cambrian Ara Salt from the South Oman salt basin. AAPG Bulletin 91, 1541–1557.
Spiers, C.J., Urai, J., Lister, G.S., Boland, J.N., Zwart, H.J., 1986. The Influence of Fluid-rock Interaction on the Rheology of Salt Rock and on Ionic Transport in the Salt. University of Utrecht, pp. 132.
Stipp, M., Kunze, K., 2008. Dynamic recrystallization near the brittle-plastic transition in naturally and experimentally deformed quartz aggregates. Tectonophysics 448, 77–97.
Stipp, M., Stünitz, H., Heilbronner, R., Schmid, S.M., 2002. The eastern Tonale fault zone: a 'natural laboratory' for crystal plastic deformation of quartz over a temperature range from 250 to 700 °C. Journal of Structural Geology 24, 1861–1884.
Tarantola, A., Diamond, L.E., Stünitz, H., 2010. Modification of fluid inclusions in quartz by deviatoric stress I: experimentally induced changes in inclusion shapes and microstructures. Contributions to Mineralogy and Petrology. doi:10.1007/s00410-010-0509-z.
Tullis, J., Yund, R.A., 1982. Grain growth kinetics of quartz and calcite aggregates. Journal of Geology 90, 301.
Underwood, E.E., 1970. Quantitative Stereology. Addison-Wesley Publishing Company.
Urai, J.L., 1983. Water assisted dynamic recrystallization and weakening in polycrystalline bischofite. Tectonophysics 96, 125–157.
Urai, J.L., Spiers, C.J., Zwart, H.J., Lister, G.S., 1986. Weakening of rock salt by water during long-term creep. Nature 324, 554–557.
Vityk, M.O., Bodnar, R.J., Doukhan, J.-C., 2000. Synthetic fluid inclusions. XV. TEM investigation of plastic flow associated with re-equilibration of fluid inclusions in natural quartz. Contributions to Mineralogy and Petrology 139, 285–297.
Wagner, T., Boyce, A.J., Erzinger, J., 2010. Fluid-rock interaction during formation of metamorphic quartz veins: a REE and stable isotope study from the Rhenish Massif, Germany. American Journal of Science 310.
Wagner, T., Cook, N.J., 2000. Late-orogenic alpine-type (apatite)-quartz fissure vein mineralization in the Rheinisches Schiefergebirge, NW Germany: mineralogy, formation conditions and lateral-secretionary origin. Mineralogical Magazine 64, 539–560.
Walte, N.P., Bons, P.D., Passchier, C.W., 2005. Deformation of melt-bearing systems – insight from in situ grain-scale analogue experiments. Journal of Structural Geology 27, 1666–1679.
Watanabe, T., Peach, C.J., 2002. Electrical impedance measurement of plastically deforming halite rocks at 125° C and 50 MPa. Journal of Geophysical Research 107 ECV 2-1–2-12.
Watson, E.B., Brenan, J.M., 1987. Fluids in the lithosphere; 1, Experimentally-determined wetting characteristics of CO_2–H_2O fluids and their implications for fluid transport, host-rock physical properties, and fluid inclusion formation. Earth and Planetary Science Letters 85, 497.
Weber, K., 1960. The structural development of the Rheinische Schiefergebirge. Geologie en Mijnbouw 60, 149–159.
Wilkins, R.W.T., Barkas, J.P., 1978. Fluid inclusions, deformation and recrystallization in granite Tectonites. Contributions to Mineralogy and Petrology 65, 293–299.
Zheng, Z., Zhang, J., Huang, J.Y., 1996. Observations of microstructure and reflectivity of coal graphites for two locations in China. International Journal of Coal Geology 30, 277–284.